IEICE TRANS. FUNDAMENTALS, VOL.E85–A, NO.1 JANUARY 2002

PAPER

Chaotic Wandering and Its Analysis in Simple Coupled Chaotic Circuits

Yoshifumi NISHIO[†a)] *and* **Akio USHIDA**[†b)], ***Regular Members***

SUMMARY In this paper, four coupled chaotic circuits generating four-phase quasi-synchronization of chaos are proposed. By tuning the coupling parameter, chaotic wandering over the phase states characterized by the four-phase synchronization occurs. In order to analyze chaotic wandering, dependent variables corresponding to phases of solutions in subcircuits are introduced. Combining the variables with hysteresis decision of the phase states enables statistical analysis of chaotic wandering.
key words: *chaos, chaotic wandering, chaos synchronization, chaotic circuits*

1. Introduction

Spatiotemporal phenomena observed in coupled chaotic networks, namely coupled systems of many chaotic cells, have attracted many researchers' attention. The studies on coupled chaotic networks are classified into two categories; discrete-time systems and continuous-time systems. For discrete-time mathematical models, there have been numerous excellent results. Kaneko's coupled map lattice is the most interesting and well-studied system [1]. He discovered various nonlinear spatiotemporal chaotic phenomena such as clustering, Brownian motion of defects and so on. Also Aihara's chaos neural network is the most important chaotic network from an engineering point of view [2]. His study indicated a new possibility for engineering applications of chaotic networks, namely dynamical search of patterns embedded in neural networks utilizing chaotic wandering. Furthermore, the application of chaos neural networks to optimization problems is widely studied ([3] and references therein). On the other hand, for continuous-time systems, several results on arrays of Chua's circuits have been reported (e.g. some papers in [4]). However, many of these studies treated only parameter values for which an isolated chaotic cell does not generate a chaotic attractor; namely only multiple stable sinks or multiple stable limit cycles. Hence, the main subject of many studies has been the wave propagation phenomenon observed for a given set of initial patterns and there are few studies on spatial patterns observed after vanishing effects of the initial patterns. Namely, the pattern switching phenomenon caused by chaotic wandering, as observed in Aihara's discrete-time chaos neural network, has not yet been studied well in continuous-time network models. Therefore, in order to fill the gap between studies of discrete-time mathematical abstract systems and studies of continuous-time real physical systems, it is important to investigate simple continuous-time coupled chaotic circuits generating chaotic wandering, clustering, pattern switching, and so on.

The authors have proposed continuous-time coupled chaotic circuit systems and have investigated the generation of spatial patterns and chaotic wandering of spatial patterns [5]. Chaotic wandering in the case of coexistence of asymmetric attractors [6] and control of generating spatial patterns [7] have been also investigated. An important feature of the coupled circuits was their coupling structure. Namely, four adjacent chaotic circuits were coupled by one resistor. Because such a coupling exhibited quasi-synchronization with phase difference [8], [9], various spatial patterns could be generated. This would be followed by the generation of several complicated spatiotemporal chaotic phenomena similar to those observed in discrete-time mathematical models. Therefore, the network based on the coupled circuits would be a good model to clarify the physical mechanism of spatiotemporal chaotic phenomena in continuous-time systems. However, because it is extremely difficult to treat higher-dimensional nonlinear phenomena in continuous-time systems theoretically, we have to develop several tools to reveal the essence of the complicated phenomena.

In this paper, four-phase quasi-synchronization of chaos and chaotic wandering over the phase states characterized by the quasi-synchronization are reported to be observed in simple coupled chaotic circuits. Although the circuits in this paper are similar to those proposed in [5], generating four-phase quasi-synchronization is more stable and easier to deal with than the two types of quasi-synchronizations reported in [5], which were almost impossible to analyze. Furthermore, statistical analysis using dependent variables corresponding to phases of the solutions in subcircuit is carried out. We will be faced with a problem where the first result will not describe the actual phenomenon well. Careful investigation of the phase states reveals that numerous inadequate decisions during transitions

Manuscript received February 28, 2001.
Final manuscript received August 20, 2001.
[†]The authors are with the Faculty of Engineering, Tokushima University, Tokushima-shi, 770-8506 Japan.
a) E-mail: nishio@ee.tokushima-u.ac.jp
b) E-mail: ushida@ee.tokushima-u.ac.jp

cause the unexpected result. In order to avoid the inadequate decisions, two methods are introduced; introductions of intermediate phase states and hysteresis decision. Computer simulated results show that the hysteresis decision makes the statistical analysis more reliable. Various characteristics of the chaotic wandering will be clarified through the analysis.

2. Circuit Model

Figure 1 shows the circuit model. In the circuit, four identical chaotic circuits are coupled by one resistor R. Each subcircuit is a three-dimensional autonomous one and consists of three memory elements, one linear negative resistor and one diode. We can regard the diodes as purely resistive elements, because their operation frequency is not too high. The coupling structure is symmetric in the sense that the exchange of any two subcircuits does not cause any change of the system structure. Also the coupling is complete in the sense that a signal of one subcircuit can reach the others without passing through the rest.

At first, the i-v characteristics of the diodes are approximated by two-segment piecewise-linear functions as

$$v_d(i_k) = \frac{1}{2}\left(r_d\, i_k + E - |\, r_d\, i_k - E\,|\right). \tag{1}$$

By changing the variables and parameters,

$$I_k = \sqrt{\frac{C}{L_1}}E\,x_k, \quad i_k = \sqrt{\frac{C}{L_1}}E\,y_k, \quad v_k = E\,z_k,$$

$$t = \sqrt{L_1 C}\,\tau, \quad \alpha = \frac{L_1}{L_2}, \quad \beta = r\sqrt{\frac{C}{L_1}},$$

$$\gamma = R\sqrt{\frac{C}{L_1}}, \quad \delta = r_d\sqrt{\frac{C}{L_1}}, \tag{2}$$

the normalized circuit equations are given as

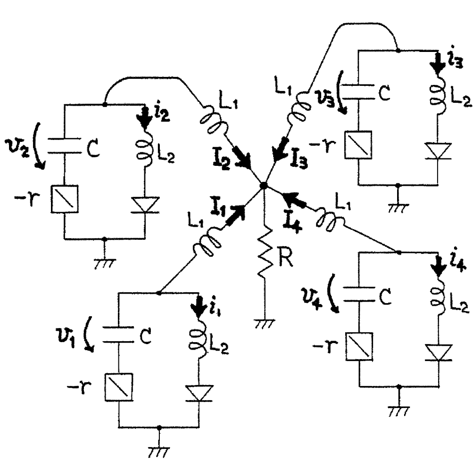

Fig. 1 Circuit model.

$$\begin{cases} \dfrac{dx_k}{d\tau} = \beta(x_k + y_k) - z_k - \gamma \displaystyle\sum_{j=1}^{4} x_j \\ \dfrac{dy_k}{d\tau} = \alpha\{\beta(x_k + y_k) - z_k - f(y_k)\} \\ \dfrac{dz_k}{d\tau} = x_k + y_k \end{cases}$$
$$(k = 1, 2, 3, 4) \tag{3}$$

where

$$f(y_k) = 0.5\,(\delta\, y_k + 1 - |\,\delta\, y_k - 1\,|\,). \tag{4}$$

Note that when the coupling parameter γ, which is in proportion to R, is equal to zero, the coupling term in (3) vanishes. Figure 2 shows a typical example of chaotic attractors observed from the isolated subcircuit. Throughout this paper, let us fix all of the circuit parameters except the coupling parameter (γ and R) for each subcircuit to produce the chaotic attractor in Fig. 2; α=7.0, β=0.14 and δ=100.0 for computer calculations and L_1=100.7 mH, L_2=10.31 mH, C=34.9 nF and r=334 Ω for circuit experiments. Moreover, for all of the computer calculations, the fourth-order Runge-Kutta method is used with step size $h = 0.005$.

3. Four-Phase Quasi-Synchronization of Chaos and Chaotic Wandering

We can observe four-phase quasi-synchronization of chaos from the coupled circuits for a relatively wide range of γ (or R). Because of chaotic oscillations, the signals cannot synchronize completely. But we can clearly see that the signals from the four subcircuits are synchronized with about 90° phase differences. Figures 3 and 4 show an example of the observed four-phase quasi-synchronizations of chaos. In the figures the phase differences of x_2, x_3 and x_4 with respect to x_1 are almost 90°, 180° and 270°, respectively.

Because of the symmetry of the coupling structure,

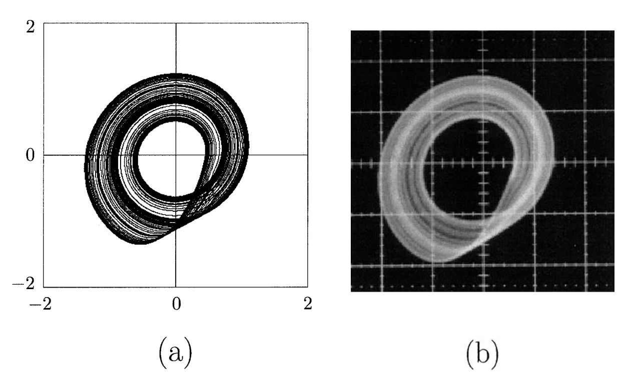

(a) (b)

Fig. 2 Typical example of chaotic attractors observed from each subcircuit. (a) Computer calculated result. x_k vs. z_k. α=7.0, β=0.14, γ=0.0 and δ=100.0. (b) Circuit experimental result. I_k vs. v_k. L_1=100.7 mH, L_2=10.31 mH, C=34.9 nF, r=334 Ω and R=0.0 Ω. H: 0.8 mA/div. V: 1.3 V/div.

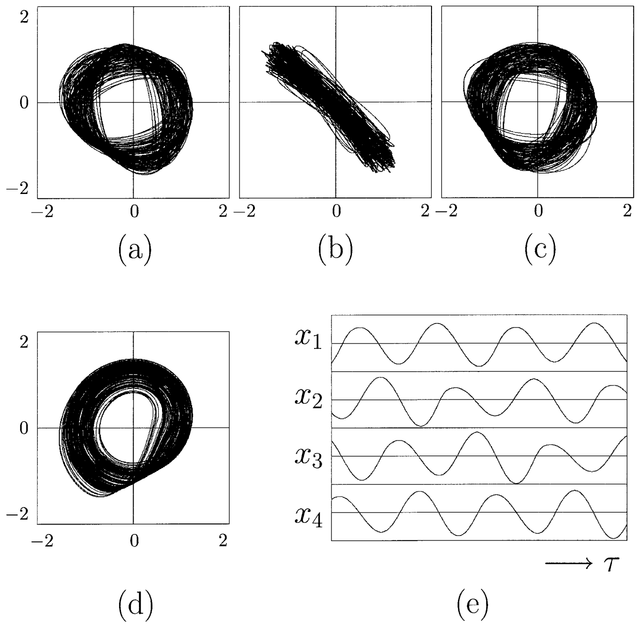

Fig. 3 Four-phase quasi-synchronization of chaos (computer calculated result). γ=0.30. (a) x_1 vs. x_2. (b) x_1 vs. x_3. (c) x_1 vs. x_4. (d) x_1 vs. z_1. (e) Time waveforms.

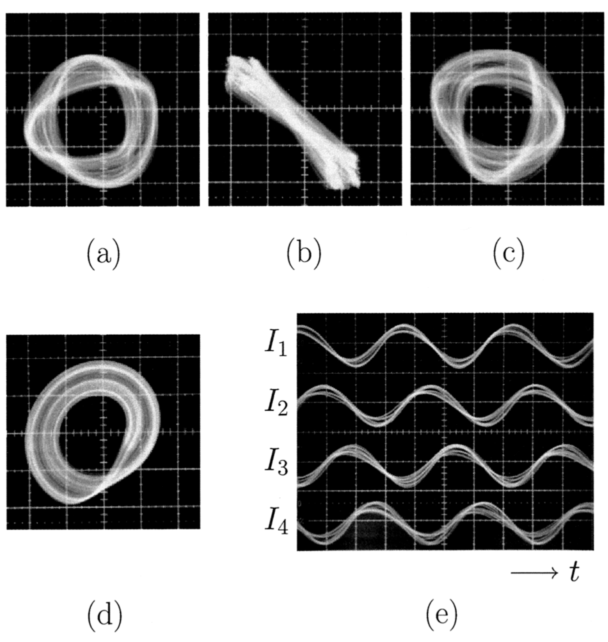

Fig. 4 Four-phase quasi-synchronization of chaos (circuit experimental result). R=198 Ω. (a) I_1 vs. I_2. (b) I_1 vs. I_3. (c) I_1 vs. I_4. (d) I_1 vs. v_1. (e) Time waveforms. (a)–(c) 0.8 mA/div. (d) H: 0.8 mA/div. V: 1.3 V/div. (e) H: 0.1 msec/div. V: 2.0 mA/div.

six different combinations of phase states coexist;

$$\begin{aligned} &S_1\colon (0°, 90°, 180°, 270°),\\ &S_2\colon (0°, 90°, 270°, 180°),\\ &S_3\colon (0°, 180°, 90°, 270°),\\ &S_4\colon (0°, 180°, 270°, 90°),\\ &S_5\colon (0°, 270°, 90°, 180°),\\ &S_6\colon (0°, 270°, 180°, 90°). \end{aligned} \tag{5}$$

Note that one subcircuit should be a reference for the phase difference since the system is autonomous. It is easy to observe all of the phase states in (5) by giving proper initial conditions. (For circuit experiments, we may have to repeat the on and off switching operations of our power supply several times before we observe all of the phase states.)

On increasing γ (or R), we can observe chaotic wandering over the six phase states of the four-phase quasi-synchronization. For such parameter values, all of the six phase states become unstable and the solution starts wandering over the six phase states. Although the wandering speed depends significantly on the parameter value, we could observe in the circuit experiments that one phase state switches to another within one second or after 10 seconds. The wandering is truly chaotic, i.e. we cannot predict when the next switching will occur or which phase state will appear next.

In order to show that the chaotic wandering exists in the circuit, let us define the Poincaré section as $z_1 = 0$ and $x_1 < 0$ and plot the values of x_k (k=1, 2, 3, 4) on $x_k - n$ (n denotes the number of iterations of the Poincaré map) plane when the solution hits the Poincaré section. Figure 5(a) shows time series $x_k(n)$ corresponding to the four-phase quasi-synchronization of chaos in Figs. 3 and 4, while Fig. 5(b) corresponds to chaotic wandering. In Fig. 5(a), each x_k remains in a certain range, while in Fig. 5(b), we can see x_k often changes its range in a complicated manner. Note that x_1 always remains in a certain range, because of the definition of the Poincaré map. In the following analysis, all of the results are based on the data on the Poincaré map obtained by computer simulations.

4. Analysis of Chaotic Wandering

4.1 Introduction of Phase Variables

Although one can see that the phase states in Fig. 5(b) switch in an irregular manner, it is almost impossible to understand the generating phenomenon completely. Therefore, we introduce the following independent variables from the discrete data of $x_k(n)$ and $z_k(n)$ on the Poincaré map.

$$\varphi_k(n) = \begin{cases} \pi - \tan^{-1} \dfrac{z_{k+1}(n)}{x_{k+1}(n)} \\ \qquad x_{k+1}(n) \geq 0 \\ -\tan^{-1} \dfrac{z_{k+1}(n)}{x_{k+1}(n)} \\ \qquad x_{k+1}(n) < 0 \text{ and } z_{k+1}(n) \geq 0 \\ 2\pi - \tan^{-1} \dfrac{z_{k+1}(n)}{x_{k+1}(n)} \\ \qquad x_{k+1}(n) < 0 \text{ and } z_{k+1}(n) < 0 \end{cases}$$

$$(k = 1, 2, 3.) \tag{6}$$

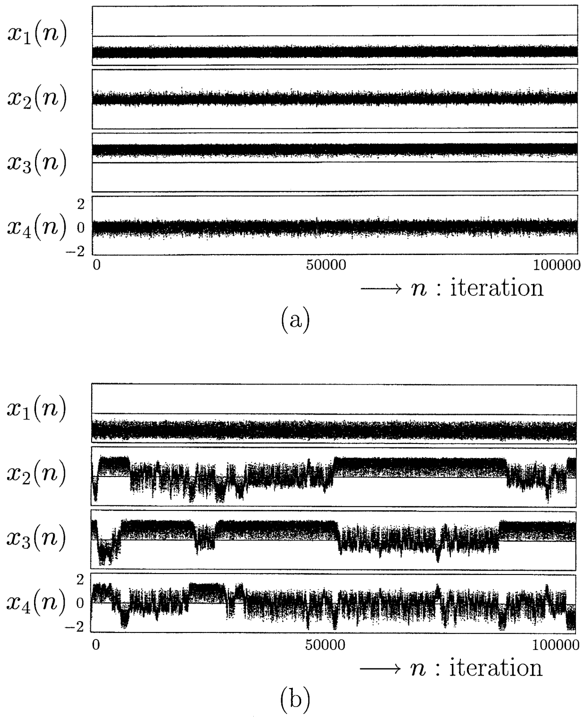

Fig. 5 Time series $x_k(n)$. (a) Four-phase quasi-synchronization of chaos. γ=0.30. (b) Chaotic wandering over different phase states of four-phase synchronizations. γ=0.46.

Because the attractor observed from each subcircuit is strongly constrained onto the plane $y_k = 0$ when the diode is off, these variables can correspond to the phase differences between the subcircuit 1 and the others. (Note that the argument of the point $(x_1(n), z_1(n))$ is always π, because of the definition of the Poincaré map.)

Figure 6 shows the time evolution of $\varphi_k(n)$ calculated from the data in Fig. 5. In Fig. 6(a), $\varphi_1(n)$ is always around $\pi/2$, $\varphi_2(n)$ is always around π and $\varphi_3(n)$ is always around $3\pi/2$, while in Fig. 6(b), $\varphi_k(n)$ changes its range in a complicated manner.

Using the independent variables in (6), we can give a precise definition of the six phase states in (5) as follows,

$$
\begin{aligned}
&S_1\colon \varphi_1 < \varphi_2 < \varphi_3,\\
&S_2\colon \varphi_1 < \varphi_3 < \varphi_2,\\
&S_3\colon \varphi_2 < \varphi_1 < \varphi_3,\\
&S_4\colon \varphi_2 < \varphi_3 < \varphi_1,\\
&S_5\colon \varphi_3 < \varphi_1 < \varphi_2,\\
&S_6\colon \varphi_3 < \varphi_2 < \varphi_1.
\end{aligned}
\tag{7}
$$

This makes it possible to decide in which phase states the solution lies. This could be very useful for statistical analysis of chaotic wandering. For example, we can check when switchings of one phase state to another occur, we can count how many switchings occur in a certain time interval, and so on.

Figure 7 shows how many switchings of phase

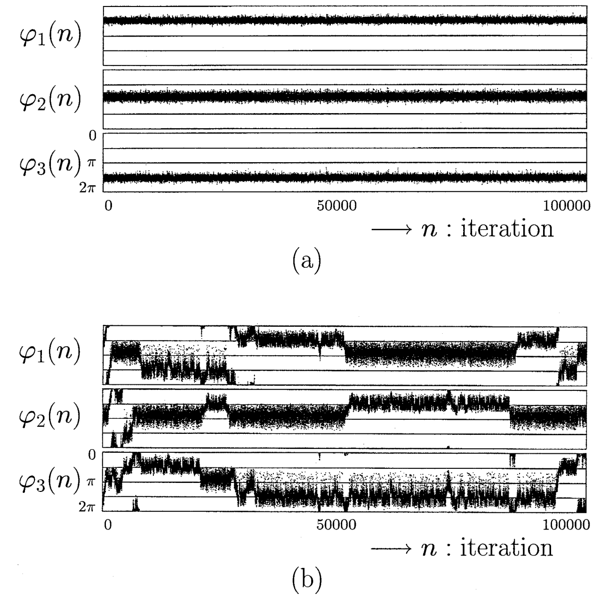

Fig. 6 Time series $\varphi_k(n)$ calculated from the data in Fig. 5. (a) Four-phase quasi-synchronization of chaos. γ=0.30. (b) Chaotic wandering over different phase states. γ=0.46.

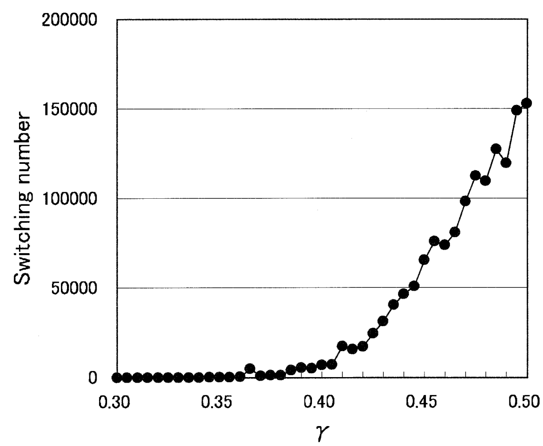

Fig. 7 Switching number during one million iterations.

states occur during one million iterations of the Poincaré map. The horizontal axis shows the coupling parameter γ. As we can see, a large number of switchings are counted for $\gamma > 0.45$. Namely, for example, at $\gamma = 0.47$ one switching occurs in every 10 iterations on average. This number is too large and the result does not describe the actual phenomenon well.

In order to determine the cause, we investigate switchings in a certain interval carefully. Figure 8 shows when switchings occur along with the time series of $\varphi_k(n)$. In the figures, each vertical line in the bottom diagrams indicates one switching. Figures 8(b) and (c) are the magnifications of parts of Fig. 8(a). From the diagrams of $\varphi_k(n)$ in Fig. 8(a), we can expect the phase state in the interval [0, 4500] to be as S_5 and the phase state in the interval [6500, 15000] to be S_6. It should

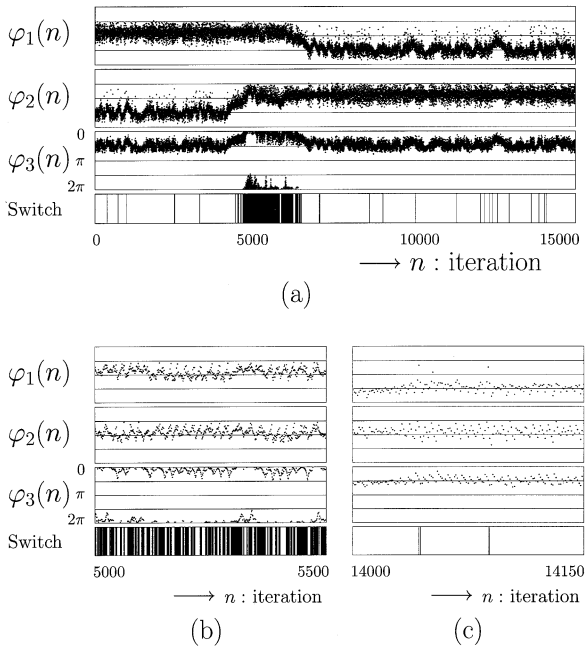

Fig. 8 Investigation of switchings of phase states. γ=0.46. (a) Switchings from S_5 to S_6. (b) Magnification during the transition. (c) Magnification indicating momentary changes.

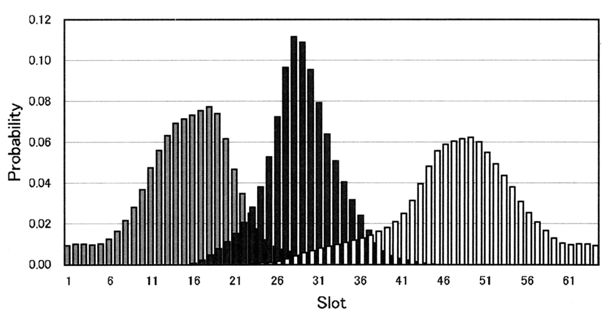

Fig. 9 Probability distribution of φ_i. Horizontal slot m indicates interval $[(m-1)\pi/32,\ m\pi/32]$. γ=0.46.

be noted that it takes a relatively long time to finish the transition in the interval [4500, 6500].

In contrast, the diagram of the switching indicates another phenomenon. Namely, from the start to the end of the transition a huge number of switchings are detected. Further, several switchings are detected in the interval without any transitions. Figure 8(b) shows that during the transition, the solution stays in the neighborhood of a hyper-plane expressed as $\varphi_1 = \varphi_2$ and $\varphi_3 = 0$. The hyper-plane corresponds to the boundary of the phase states S_1, S_3, S_5 and S_6. Hence, small fluctuations around the hyper-plane cause a large increase of the number of switchings. Figure 8(c) shows that a momentary change of φ_k causes two consecutive inadequate decisions.

Figure 9 shows the probability distribution of φ_i. In the figure interval $[0,\ 2\pi]$ is divided into 64 small intervals equally and the vertical axis indicates the probability that φ_i lies in the corresponding interval. The left group corresponds to the minimum values of φ_i and the right group corresponds to the maximum values of φ_i. We can see from the figure that the probability that φ_i remains around 0 is not small. ($\pm 30°$ almost corresponds to the slots 1–5 and 60–64.) Hence, we must consider that the situation in Fig. 8(b) occurs frequently. Namely, some methods should be applied to avoid the inadequate decisions caused by the solutions remaining around the above-mentioned hyper-planes.

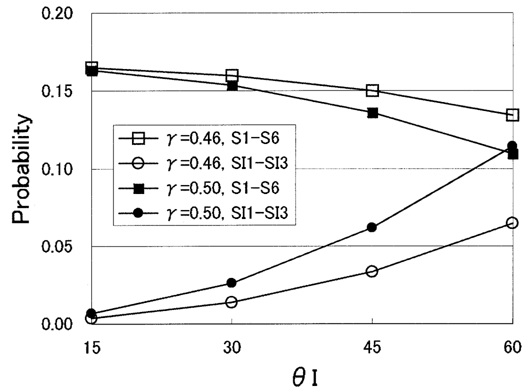

Fig. 10 Probabilities of solutions being in S_i and S_{Ii}.

4.2 Introduction of Intermediate Phase States

The number of inadequate decisions during transitions would decrease if we regarded neighborhoods of hyper-planes where the solutions stay during transitions as new phase states. Hence, the following three intermediate phase states are introduced,

$$\begin{array}{ll} S_{I1}: & \min\{2\pi-\varphi_1,\ \varphi_1\} < \theta_I\ \cap\ |\varphi_2-\varphi_3| < \theta_I \\ S_{I2}: & \min\{2\pi-\varphi_2,\ \varphi_2\} < \theta_I\ \cap\ |\varphi_1-\varphi_3| < \theta_I \\ S_{I3}: & \min\{2\pi-\varphi_3,\ \varphi_3\} < \theta_I\ \cap\ |\varphi_1-\varphi_2| < \theta_I \end{array} \tag{8}$$

where θ_I is a parameter deciding the size of the region of the intermediate phase states. Note that the conditions of the decisions corresponding to the original six phase states in (7) are modified so that their regions do not overlap with those of (8).

Figure 10 shows probabilities of the solutions being in the phase states after introducing the intermediate phase states. Each plot indicates the averaged value of the probabilities of the corresponding phase states, which are given by computer simulations (10 million iterations of the Poincaré map). As θ_I increases, the probabilities corresponding to the intermediate phase states become large. For example, for $\gamma = 0.46$ and $\theta_I = 45°$, the sum of the probabilities corresponding to the three intermediate phase states is 3×0.0335, namely the solution stays in the intermediate phase states about 10% of the total time.

Figure 11 shows how the switchings change after introducing the intermediate phase states for different

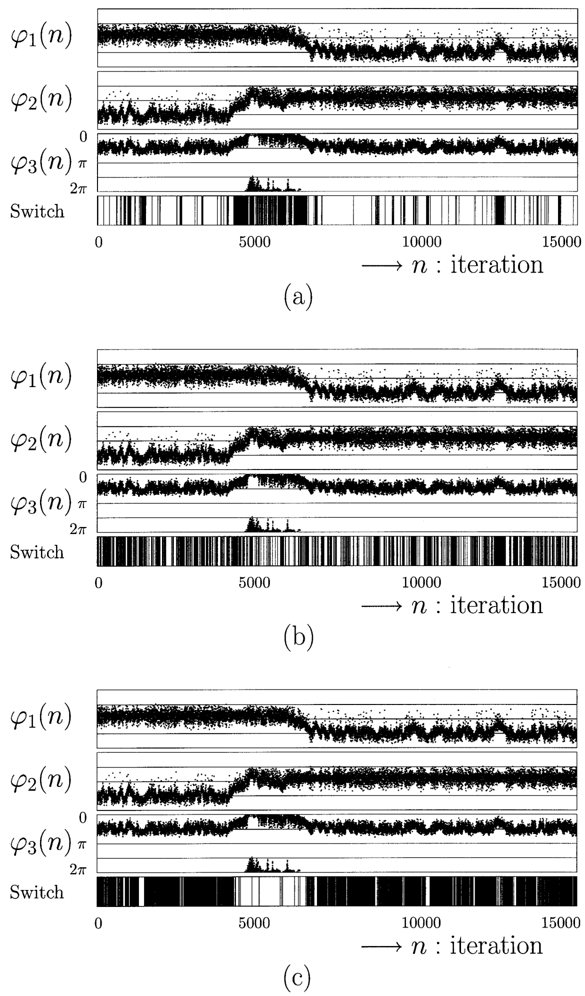

Fig. 11 Switchings of phase states with three intermediate states. γ=0.46. (a) $\theta_I = 60°$. (b) $\theta_I = 75°$. (c) $\theta_I = 90°$.

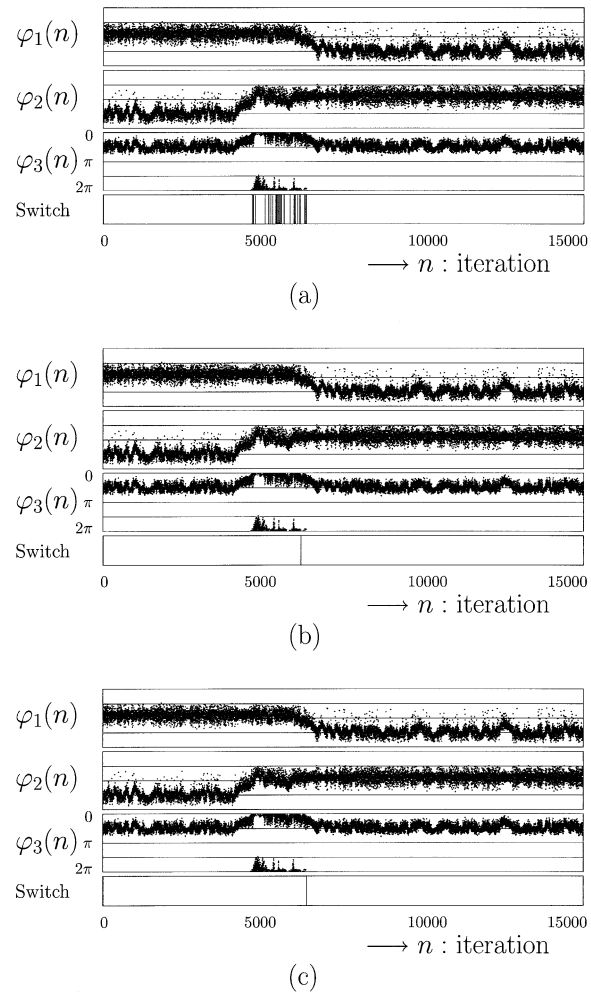

Fig. 12 Switchings of phase states with hysteresis decision. γ=0.46. (a) $\theta_H = 30°$. (b) $\theta_H = 45°$. (c) $\theta_H = 60°$.

values of θ_I. As we can see from the figures, the intermediate phase states make the situation worse with respect to the expectations. Undoubtedly, inadequate decisions during the transition (in [4500, 6500]) decrease considerably as θ_I increases. However, the switching number in the other intervals increases considerably. As a result, the total number of switchings becomes less meaningful.

We have to conclude that introducing new boundaries of the phase states causes an increase of the inadequate decisions around the new boundaries. However, the fact that the solutions stay for a relatively long time in the intermediate phase states is useful for understanding the phenomenon correctly.

4.3 Introduction of Hysteresis Decision

In order to reduce the inadequate decisions during transitions without influence on the other interval, we introduce a hysteresis feature into the decisions of the six phase states in (7). Namely, we do not count switchings if the angle between any two phases of four is smaller than θ_H. In other words, we make decisions of the phase states only if the following is satisfied;

$$\min\{\varphi_1,\ \varphi_2,\ \varphi_3,\ 2\pi-\varphi_1,\ 2\pi-\varphi_2,\ 2\pi-\varphi_3,\\ |\varphi_1-\varphi_2|,\ |\varphi_1-\varphi_3|,\ |\varphi_2-\varphi_3|\} \ >\ \theta_H \tag{9}$$

Figure 12 shows how the switchings change after introducing the hysteresis decision for different values of θ_H. We can see that even for small θ_H, the inadequate decisions decreases considerably. The hysteresis decision can eliminate the inadequate decisions by the momentary change as well as those during transitions successfully.

Figure 13 shows how the switching numbers decrease by introducing the hysteresis decision. We can observe from Fig. 13(b) that slopes of the curves change around $\theta_H = 50°$ regardless of the coupling parameter. Although the theoretical reason why the curves have the turning points has not been clarified, it may be caused by the existence of the two inadequate decisions as shown in Figs. 8(b) and (c).

Table 1 shows the probabilities of sojourn time in each phase state for different values of θ_H, which are given by computer simulations (10 million iterations of the Poincaré map). For example, for $\theta_H = 0°$ (i.e. no hysteresis decision) the probability that the sojourn time is 1 is 78.2%. This means that the solution entering a phase state will exit to another phase state after one step of the Poincaré map with probability 78.2%. Furthermore, for $\theta_H = 0°$ the probability that the sojourn time is more than 1000 is 0.1%. Clearly, this result does not explain the phenomenon correctly. (See the horizontal scale of Fig. 5.) For $\theta_H \geq 45°$, the effect of the hysteresis is clear. Especially, for $\theta_H \geq 60°$ the probability that the sojourn time is less than 100 is zero and for $\theta_H = 75°$ the probability that the sojourn time is more than 10000 is 37.8%. The distribution of these probabilities of the sojourn time is depicted in Fig. 14. The slots in the horizontal axis of the figure denote the ranges of the sojourn time and are summarized in Table 2.

Finally, Table 3 shows the averages of the sojourn time in each phase state for different values of θ_H, which are given by computer simulations. The average numbers of iterations are converted into average time using the approximated value of the period (0.36 [msec]) in Fig. 4(e). Although the corresponding data obtained from real circuit experiments are not available, the results for $\theta_H \geq 45°$ do not appear to be far from the observed phenomenon.

5. Conclusions

In this study, chaotic wandering observed in four coupled chaotic circuits has been reported and analyzed.

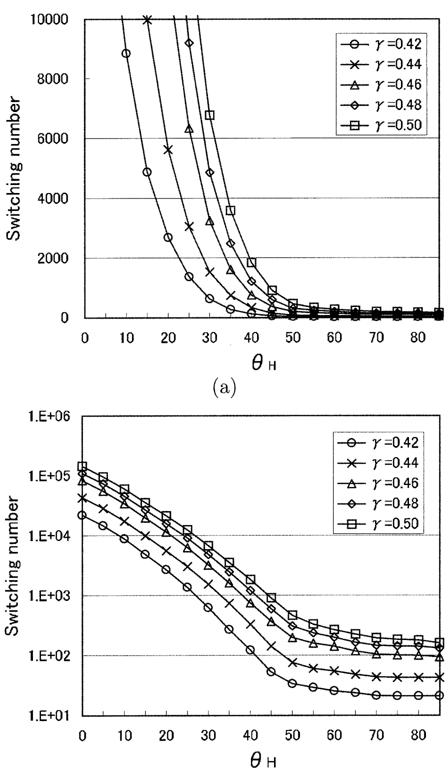

Fig. 13 Switching number with hysteresis decision. (a) Ordinary scale. (b) Logarithmic scale.

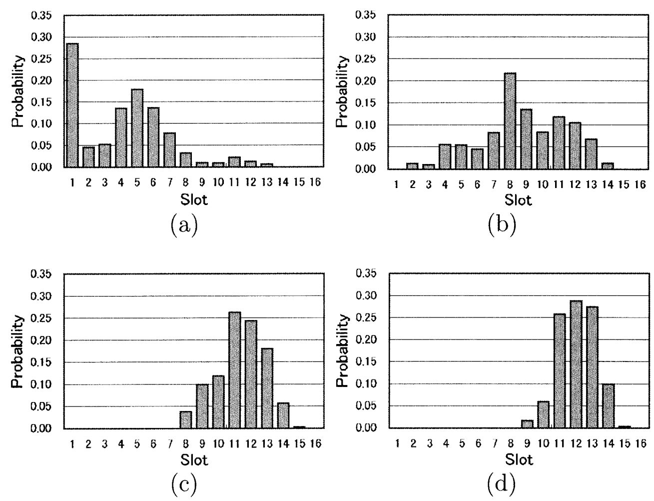

Fig. 14 Probability distribution of sojourn time. γ=0.46. Ranges of slots are in Table 2. (a) $\theta_H = 30°$. (b) $\theta_H = 45°$. (c) $\theta_H = 60°$. (d) $\theta_H = 75°$.

Table 2 Ranges of slots in Fig. 14.

Slot	Sojourn time (n)	Slot	Sojourn time (n)
1	1−2	9	501−1000
2	3−5	10	1001−2000
3	6−10	11	2001−5000
4	11−20	12	5001−10000
5	21−50	13	10001−20000
6	51−100	14	20001−50000
7	101−200	15	50001−100000
8	201−500	16	100001−∞

Table 1 Probabilities of sojourn time for different θ_H. γ=0.46.

Sojourn time (n)	θ_H					
	0°	15°	30°	45°	60°	75°
1	0.782	0.554	0.284	0.000	0.000	0.000
1–10	0.931	0.693	0.382	0.022	0.000	0.000
1–100	0.977	0.959	0.832	0.177	0.000	0.000
1–1000	0.999	0.985	0.951	0.611	0.137	0.017
1–10000	1.000	1.000	0.994	0.919	0.761	0.622
1–∞	1.000	1.000	1.000	1.000	1.000	1.000

Table 3 Average of sojourn time for different θ_H. γ=0.46.

θ_H	Average of sojourn time	
	iteration (n)	time [sec]
0°	12.0	0.00432
15°	50.4	0.0181
30°	307.9	0.111
45°	2697.8	0.971
60°	7079.2	2.55
75°	9915.9	3.57

In order to analyze chaotic wandering, dependent variables corresponding to phases of solutions in subcircuits were introduced. Combining the variables with hysteresis decision of the phase states enabled statistical analysis of chaotic wandering.

Although the results obtained by introducing the intermediate phase states were not good, we will continue to work with the idea of the intermediate phase states in the future, because the simulation results suggest that the solution stays for a long time in the intermediate phase states.

This is the first step in the statistical analysis of chaotic wandering in simple continuous-time circuits. However, we believe this result would contribute to understanding the higher-dimensional nonlinear phenomena, because the phenomenon analyzed in this paper would be observed in various other coupled chaotic circuits. At the same time, we feel that more detailed statistical analysis on the phenomenon should be carried out and more complicated phenomena in larger sized coupled circuits should also be investigated. Furthermore, some theoretical supports would make the results more reliable, though this may be difficult.

Acknowledgements

The authors would like to thank Professor Martin Hasler of the Swiss Federal Institute of Technology, Lausanne and Professor Takashi Hikihara of Kyoto University for their valuable comments.

References

[1] K. Kaneko, Theory and Applications of Coupled Map Lattices, John Wiley & Sons, Chichester, 1993.
[2] K. Aihara, T. Takabe, and M. Toyoda, "Chaotic neural networks," Phys. Lett. A, vol.144, nos.6&7, pp.333–340, 1990.
[3] L. Chen and K. Aihara, "Global searching ability of chaotic neural networks," IEEE Trans. Circuits & Syst. I, vol.46, no.8, pp.974–993, Aug. 1999.
[4] L.O. Chua, ed., "Special issue on nonlinear waves, patterns and spatio-temporal chaos in dynamic arrays," IEEE Trans. Circuits & Syst. I, vol.42, no.10, Oct. 1995.
[5] Y. Nishio and A. Ushida, "Spatio-temporal chaos in simple coupled chaotic circuits," IEEE Trans. Circuits & Syst. I, vol.42, no.10, pp.678–686, Oct. 1995.
[6] Y. Nishio and A. Ushida, "On synchronization phenomena in coupled chaotic circuits networks," Proc. 1996 IEEE International Symposium on Circuits & Syst., vol.3, pp.92–95, May 1996.
[7] Y. Nishio and A. Ushida, "Pattern control in a coupled chaotic network and its possible application in communications," Proc. 1997 IEEE International Symposium on Circuits & Syst., vol.2, pp.1037–1040, June 1997.
[8] Y. Nishio, K. Suzuki, S. Mori, and A. Ushida, "Synchronization in mutually coupled chaotic circuits," Proc. 1993 European Conference on Circuit Theory & Design, vol.1, pp.637–642, Aug. 1993.
[9] Y. Nishio and A. Ushida, "Quasi-synchronization phenomena in chaotic circuits coupled by one resistor," IEEE Trans. Circuits & Syst. I, vol.43, no.6, pp.491–496, June 1996.

Yoshifumi Nishio received the B.E., M.E., and Ph.D. degrees in electrical engineering from Keio University, Yokohama Japan, in 1988, 1990, and 1993, respectively. In 1993, he joined the Department of Electrical and Electronic Engineering at Tokushima University, Tokushima Japan, where he is currently an Associate Professor. From May 2000 he spent a year in the Laboratory of Nonlinear Systems (LANOS) at the Swiss Federal Institute of Technology Lausanne (EPFL) as a visiting professor. His research interests include analysis and application of chaos in electrical circuits, analysis of synchronization in coupled oscillators circuits, development of analyzing methods for nonlinear circuits and theory and application of cellular neural networks. Dr. Nishio is a member of the IEEE.

Akio Ushida received the B.E. and M.E. degrees in electrical engineering from Tokushima University in 1961 and 1966, respectively, and the Ph.D. degree in electrical engineering from University of Osaka Prefecture in 1974. He was an associate professor from 1973 to 1980 at Tokushima University. Since 1980 he has been a Professor in the Department of Electrical Engineering at the same university. From 1974 to 1975 he spent one year as a visiting scholar at the Department of Electrical Engineering and Computer Sciences at the University of California, Berkeley. His current research interests include numerical methods and computer-aided analysis of nonlinear system. Dr. Ushida is a member of the IEEE.